Pergamon

Int. J. Solids Structures Vol. 32, No. 6/7, pp. 857–881, 1995

0020-7683/95 $9.50 + .00

0020-7683(94)00165-0

PLANE STRESS STABLE CRACK GROWTH AND *J*-INTEGRAL/HRR FIELD

G. B. MAY and A. S. KOBAYASHI
University of Washington, Department of Mechanical Engineering, Seattle, WA 98195, U.S.A.

(*Received* 8 *December* 1993; *in revised form* 25 *April* 1994)

Abstract—Moiré interferometry with line densities of 1200 and 40 lines per mm was used to determine the two orthogonal displacements surrounding a stably extending crack in a 2024-T3 aluminum alloy, single edge cracked specimen. The test protocol consisted of using the fine moiré grating prior to and up to the onset of crack extension and the coarse moiré grating for the ensuing crack extension up to $\Delta a = 6$ mm. The displacement fields were used to compute the *J*-integrals for various contours during crack tip blunting and crack extension. As expected, the far-field *J*-integral value prior to stable crack growth coincided with the LEFM strain energy release rate *G*, and validated the experimental procedure. However, the *J* values obtained from the near tip contour increased slowly, while the far-field *J* values increased rapidly with increasing stable crack growth. The HRR displacement field was computed from the experimentally determined far-field *J*. The HRR displacement field agreed with the measured displacement field prior to stable crack growth since $J = G$. However, the HRR horizontal displacement field progressively deviated from the measured values with crack extension.

INTRODUCTION

For the past five years, the authors and their colleagues have used experimentally determined displacement fields to compute the *J*-integral directly in thin aluminum fracture specimens (Kang and Kobayashi, 1988; Dadkhah and Kobayashi, 1990, 1994; Dadkhah *et al.*, 1992; May *et al.*, 1993). The contour integration was performed using the definition of the *J*-integral (Rice, 1968) with an added assumption that the elastic–plastic response of the specimen material could be represented by a power hardening form with experimentally determined power hardening coefficients. These *J*-integral values agreed well with the corresponding elastic values under low load and with the known elastic–plastic solutions (Kumar *et al.* 1981) at higher loads prior to stable crack growth. Similar conclusions were obtained by Schultheisz (1991) who studied the effect of crack tunnelling in 10 mm thick, 4340 alloy steel, three point bend specimens. Under a small stable crack growth of 1–3 mm, however, the near-field *J*-integral values increasingly deviated from the known solutions (Kumar *et al.* 1981) and were as much as one quarter of that computed by the aforementioned EPRI elastic–plastic handbook values.

These *J*-integral values were then used to compute the HRR displacement field (Hutchinson, 1968; Rice and Rosengren, 1968) for comparison with the experimentally measured displacement. Theoretically the HRR displacement field should have coincided with the measured displacement field within the experimental and numerical error bounds. In reality, the measured and HRR displacements perpendicular to the crack, i.e. the v-displacements, agreed well but substantial differences were found in the corresponding values for the displacements parallel to the crack, i.e. the u-displacements. Attempts were also made to characterize the second order term in the asymptotic crack tip displacement field which is defined here as the difference between the measured and HRR displacements. These results suggested that neither the two parameter characterization by the *Q*-stress (O'Dowd and Shih, 1991, 1992, 1993), nor the *T*-stress (Betegon and Hancock, 1991), prevailed. Thus, without the presence of an HRR field or an HRR field with the higher order terms at the elastic–plastic crack tip, the much heralded *J*-integral loses its physical significance as the strength of the HRR singular field.

Many theoretical and numerical studies related to the J-integral and the HRR field have been published since 1968. Much of these studies were limited to computing the J-integral values for various plane strain, boundary value problems and the extent of the J-dominant region which is synonymous with the HRR field. Also higher order terms for the asymptotic stress, strain and in some cases the deformation fields for a plane crack tip field in a power hardening material were derived by Li and Wang (1986), Sharmar and Aravas (1991), Yang *et al.* (1993) and Xia and Wang (1993). Noteworthy in these theoretical analyses is the two parameter, ductile fracture criterion, which was suggested by Li and Wang (1986), based on a critical J_{IC} and a high triaxial stress ahead of a plane strain crack front. These two parameters, together with the J-integral, formed the basis of the J–Q theory of fracture (O'Dowd and Shih, 1991, 1992). More recently, Wang (1993) has shown that the cumulative sum of the higher order terms is equivalent to the triaxial stress and thus O'Dowd and Shih (1993) have redefined Q to represent the entire difference between the actual crack tip stress and the HRR singular component. For small scale yielding, the triaxiality parameter Q was related to the elastic T-stress and the J_{IC}, predicted from the J–Q ductile fracture criterion, agreed with the experimental results by Kirk *et al.* (1993).

Most of the literature discussed above was related to the state of plane strain of a stationary crack tip. The experimental investigation, which was described previously, involved a near plane stress state with an inevitable stable crack growth. This state of plane stress effectively eliminated the triaxiality constraint, which is the basis of the J–Q theory, and thus the J–Q theory is not applicable for evaluating the test results of thin fracture specimens.

A theoretical analysis of the higher order asymptotic crack tip field for a plane stress configuration has been conducted by Yang *et al.* (1993). For a power hardening coefficient of $n = 3$, their three term displacement solution predicted the u-displacement while the v-displacement required only the HRR singular component. These results are in qualitative agreement with the results of the authors and their colleagues with the exception that the HRR displacement underpredicted the measured u-displacement. In a recent note, Chao (1993a) has indicated that for a mode I plane stress state with $n > 3.2$, the higher order terms are uniquely governed by the J-integral and thus ductile fracture for such case can be characterized by a single parameter of J. This important conclusion is in qualitative agreement with the results of Dadkhah and Kobayashi (1994) who showed that throughout a stable crack growth of $\Delta a = 2.5$ mm, the v-displacements, were uniquely represented by the J-integral values, in the 2024-0 aluminum alloy, single edge notched (SEN) specimens and the biaxially and uniaxially loaded cruciform specimens. Moreover Chao (1993b) has shown that the u-component of the crack tip displacement approaches the HRR field with increasing biaxiality. Again, this theoretical analysis is in qualitative agreement with the experimental results by Dadkhah and Kobayashi (1994).

The above brief review indicates that further theoretical and experimental analyses are needed before the two parameter fracture criterion such as the J–Q or J–T theory can be applied to a plane stress fracture specimen. A more important consequence is that J is no longer a path independent integral in the presence of a small crack extension, such as $\Delta a = 3$ mm which is unavoidable in a high temperature environment, especially in the presence of creep.

TWO PARAMETER CRACK TIP STATE

The high order asymptotic elastic–plastic crack tip stress field by Li and Wang (1986), Sharma and Aravas (1991) and Yang *et al.* (1993) is based on the J_2 deformation theory with the following power hardening material of Ramberg–Osgood:

$$\varepsilon_{ij} = \frac{1+\nu}{E} s_{ij} + \frac{1-2\nu}{3E} \sigma_{kk} \delta_{ij} + \tfrac{3}{2} \alpha \varepsilon_0 \left(\frac{\sigma_e}{\sigma_0} \right)^{n-1} \frac{s_{ij}}{\sigma_0} \tag{1}$$

where $j = 1$ or 2 corresponds to a Cartesian coordinate system with axes parallel or

perpendicular to the crack, respectively; E and ν are the modulus of elasticity and Poisson's ratio, respectively; σ_0 and ε_0 are the yield stress and strain, respectively; α and n are material constants; σ_e and s_{ij} are the equivalent and deviatoric stress, respectively.

For a plane stress state, Hom *et al.* (1994) has shown that the two term representation of the asymptotic crack tip field, in polar coordinates, can be represented at the crack tip as

$$u_i(r,\theta) = \alpha\varepsilon_0 r\left(\frac{J}{\alpha\varepsilon_0\sigma_0 I_n r}\right)^{n/(n+1)} u_{i1}(\theta,n) + \varepsilon_0 r\left(\frac{J}{\alpha\varepsilon_0\sigma_0 I_n r}\right)^{1/(n+1)} u_{i2}(\theta,n)$$

$$\varepsilon_{ij}(r,\theta) = \alpha\varepsilon_0\left(\frac{J}{\alpha\varepsilon_0\sigma_0 I_n r}\right)^{n/(n+1)} \varepsilon_{ij1}(\theta,n) + \varepsilon_0\left(\frac{J}{\alpha\varepsilon_0\sigma_0 I_n r}\right)^{1/(n+1)} \varepsilon_{ij2}(\theta,n)$$

$$\sigma_{ij}(r,\theta) = \sigma_0\left(\frac{J}{\alpha\varepsilon_0\sigma_0 I_n r}\right)^{1/(n+1)} \sigma_{ij1}(\theta,n) + \frac{\sigma_0}{\alpha}\left(\frac{J}{\alpha\varepsilon_0\sigma_0 I_n r}\right)^{(2-n)/(n+1)} \sigma_{ij2}(\theta,n) \tag{2}$$

where

$$J = \int_\Gamma [W\,\mathrm{d}x_2 - \sigma_{ij} n_j u_{i,1}\,\mathrm{d}s] \tag{3}$$

and the strain energy density

$$W = \int_\varepsilon \sigma_{ij}\,\mathrm{d}\varepsilon_{ij}, \tag{4}$$

$i,j = 1,2$ corresponds to a Cartesian coordinate system with its origin at the crack tip; nj represents a unit vector normal to any contour which encloses the crack tip u_{i1}, u_{i2}; ε_{ij1}, ε_{ij2}, σ_{ij1} and σ_{ij2} are tabulated angular functions (Yang *et al.*, 1993; Shih, 1983) of the polar coordinate θ and the hardening exponent n, and I_n is a tabulated constant (Shih 1983).

Equations (1), (3) and (4) can be used to evaluate directly the J-integral from the measured displacement field along rectangular contours which encompass the crack tip. First the strain field at each loading stage is computed from the measured displacement field at a given point on the contour. Then the corresponding stress is computed from eqn (1) and, together with the measured strain, the strain energy density is determined. Details of this analysis, which is based on the deformation theory of plasticity and which was also the basis of the original definition of J-integral (Rice, 1968), and the numerical integration procedure are given in Kang and Kobayashi (1988).

The J-integral value determined above was then substituted into eqn (2) to compute the HRR singular displacement terms. The second order term could not be computed since the corresponding u_{i2} was not given in Yang *et al.* (1993). Assuming that the second order term is much larger than the sum of the remaining higher order terms, an indirect check on the second order term can be made by noting that it varies as $r^{n/(n+1)}$.

EXPERIMENTAL ANALYSIS

Experimental procedure

The orthogonal displacement components surrounding the crack tip were measured via moiré interferometry using two specimens, each with a different grating. The first specimen was coated with a fine, cross diffraction grating of 1200 lines/mm and was used in the initial phase of loading prior to stable crack growth. The second specimen was coated with a relatively coarse, cross diffraction grating of 40 lines/mm and was used to record the crack displacement after stable crack growth commenced. This coarse grating was necessary due to the gross yielding and the large strain components, which generated a moiré fringe pattern too dense to resolve, associated with the large stable crack growth in a ductile

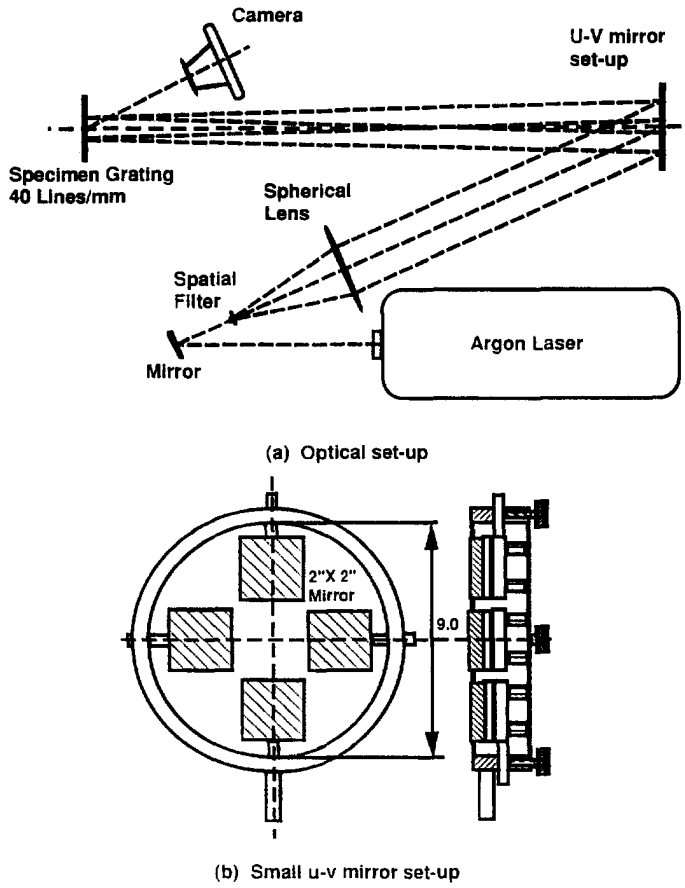

Fig. 1. Moiré interferometer set-up for 40 lines/mm grating.

specimen. The fine, cross diffraction grating was transferred using the procedure of Post (1993). The coarse, crossed diffraction grating was transferred onto the specimen surface using photoresist and is similar to the procedure developed by Ifju and Post (1991). However, in this study, the highly polished surface of the aluminum specimen provided sufficient reflectivity and thus an evaporated aluminized coating was not used. This reflective specimen surface also eliminated the loss of moiré fringes at high strain where an aluminized coating may craze and obliterate the diffraction grating.

The specimen was illuminated by a four-beam moiré interferometer for simultaneous recording of the two orthogonal displacement fields (Guo and Kobayashi, 1994). Figure 1 shows a special four-beam moiré interferometer set-up for low frequency grating, which can record the moiré fringes in a severely warped specimen surface, such as that at the crack tip. The coarse diffraction grating reduced the incident angle of the four beams thus simplifying the u–v mirror supports. Moiré interferometry fringes are then generated by the two coherent beams which are projected on to the deep diffraction grating on the specimen surface and which interfere with the radiated diffracted beam. These fringes are visible from all directions and thus a good contrast of the moiré fringes in the crack tip plastic zone is obtained even when the specimen is warped.

Specimen

The specimen consisted of a fatigue precracked, thin single edge notch (SEN), 2024-T3 aluminum alloy specimen shown in Fig. 2. The moiré diffraction grating covered a region of 25.4×50.8 mm surrounding the crack as shown. Also shown schematically are the integration contours. Figure 3 shows the uniaxial stress–strain relations for two directions, i.e. parallel and perpendicular to the rolling direction of the sheet. Also shown is the average of the two relations and the two power hardening coefficients and the least square

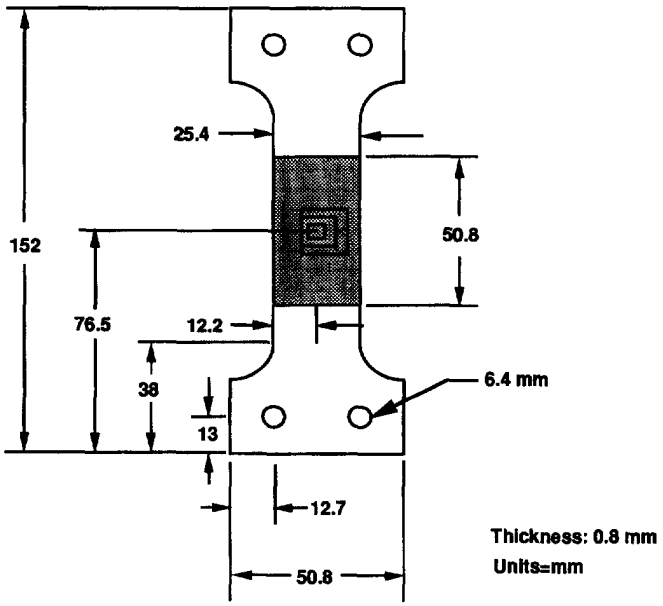

Fig. 2. SEN aluminum alloy specimen with J contours shown.

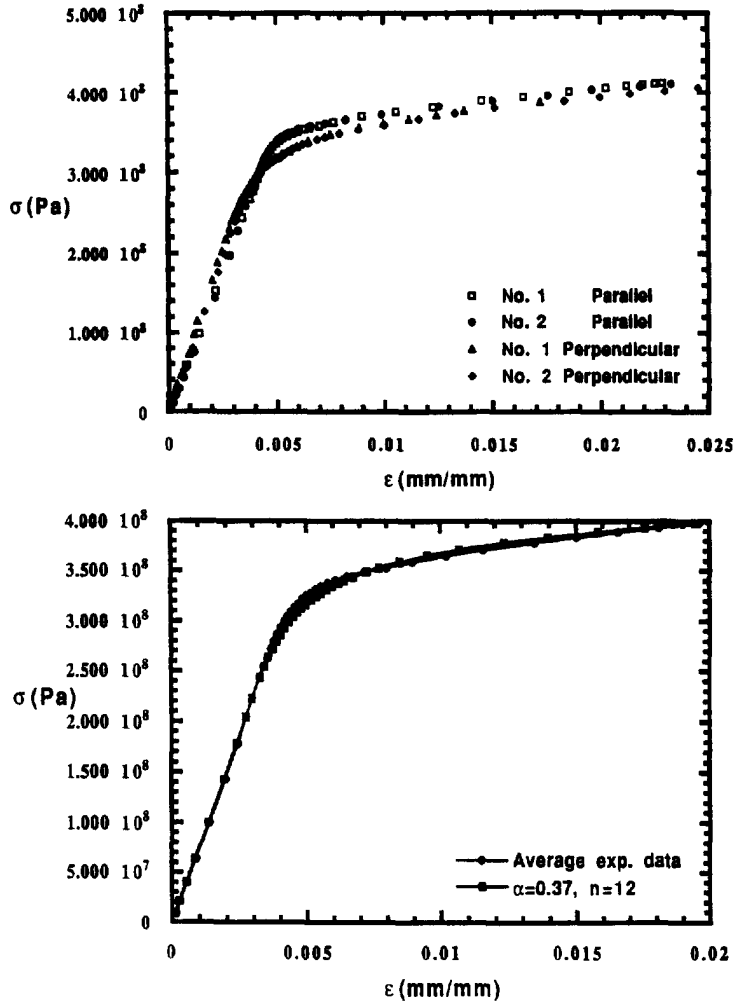

Fig. 3. Uniaxial stress–strain curve for 2024-T3.

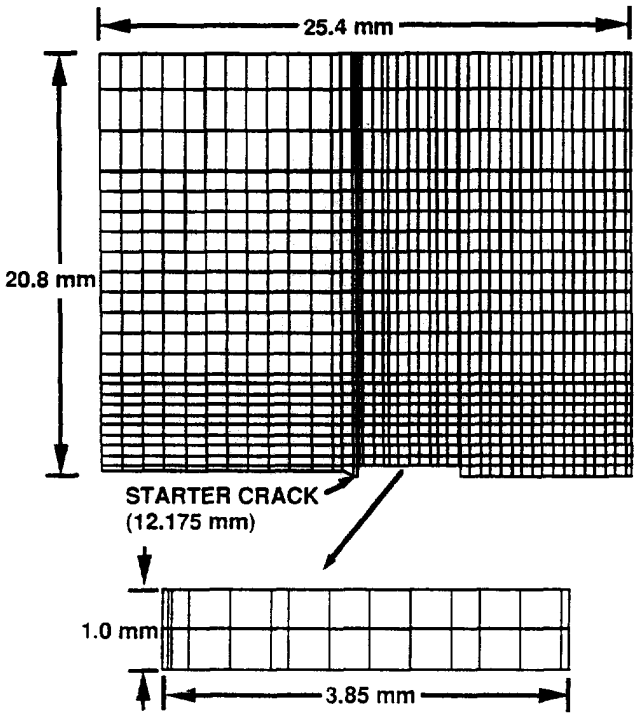

Fig. 4. Finite element mesh used in elastic–plastic analysis.

fitted σ–ε relation (Dadkhah and Kobayashi, 1990). The SEN specimen was subjected to uniaxial tensile loading in a displacement controlled testing machine and the moiré interferometry patterns were recorded at various stages of stable crack growth.

NUMERICAL ANALYSIS

A commercial finite element code was used to compute the elastic–plastic state associated with the stable crack growth in this specimen. The objective of this numerical analysis was to generate results, which can be compared with the experimental results, at various stages of stable crack growth with large scale yielding.

Unlike the traditional finite element (FE) analysis, the measured displacements near the boundary of the moiré grating were used as input boundary conditions to the FE model of the SEN specimen. As discussed by Hareesh and Chiang (1988) and Sivaneri *et al.* (1991), this procedure not only resulted in saved computer time but provided detailed information, which is lacking in the moiré analysis particularly at the initial stage of stable crack growth, in the immediate vicinity of the crack tip. Also, as described in Hareesh and Chiang (1988), this load path dependent, elastic–plastic finite element analysis must start from an early stage of plastic yielding and proceed incrementally along the loading path.

Figure 4 shows the two-dimensional, plane stress finite element model used in this analysis. The power hardening stress–strain relation in this incremental elastic–plastic analysis was that of Dadkhah and Kobayashi (1990). Due to the sensitivity of the FE method to displacement prescribed boundary conditions, a second order curve, which was fitted to the measured boundary displacements obtained from moiré interferometry, constituted the input boundary condition.

RESULTS

Eleven increments of load, i.e. five increments for the specimen with a fine moiré gratings and six increments for the specimen with a coarse grating, were applied and the

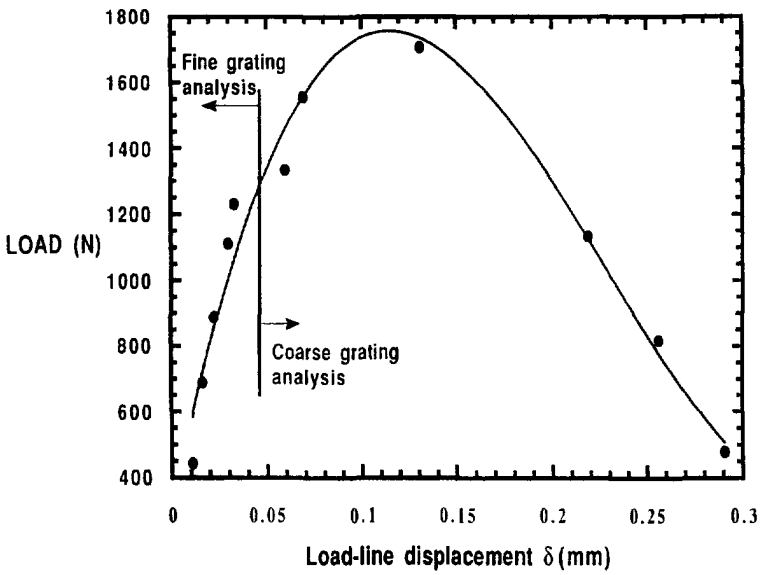

Fig. 5. Load history of two 2024-T3 SEN specimens.

corresponding moiré interferometry fringes were recorded. Figure 5 shows the measured load versus the computed load line displacement for the two specimens with the fine and the coarse gratings. The continuity in the two relations justifies the use of the two specimens in this study. The J values were then computed along three contours of 10 mm × 10 mm, 15 mm × 15mm and 17.5 mm × 25 mm for each increment of loading.

Figures 6(a) and (b) show typical moiré fringe patterns corresponding to the displacement parallel u, and perpendicular v, to the crack using the fine and coarse diffraction gratings, respectively. The offset in the crack path in Fig. 6(b) is due to shear lip which forms immediately with crack extension. Also shown in Figs 6(a) and (b) are the rectangular contours used for the J-integral computation. This computation for the specimen with a coarse diffraction grating, using moiré interferometry data, was conducted during the later stage of loading which yielded denser moiré fringe patterns.

Figures 7(a), (b) and (c) show a comparison of the various J values of interest. J_{FEM} designates the value of the J-integral computed by the commercial FE code, using the moiré fringe data as input boundary conditions, prior to and with crack extension. J_{LEFM} was computed by $J = G$ (strain energy release rate) $= K_I^2/E$ where K_I was obtained from the stress intensity factor listing in Tada *et al.* (1973) and E is the initial elastic modulus. J_{SHIH} was obtained using the procedure and tables of Kumar *et al.* (1981). J values were also obtained using an algorithm which calculated the value of the J-integral along a designated integration contour on the moiré fringe pattern. $J_{EXPERIMENTAL}$ is the value of J associated with the largest contour. Figure 7(a) shows that the $J_{EXPERIMENTAL}$ is in good agreement with J_{LEFM} at lower loading, or in the presence of small scale yielding, as expected. The two J values increasingly differ at a higher loading where large scale yielding prevails prior to stable crack growth. Figure 7(b) shows that the value of $J_{EXPERIMENTAL}$ is close to the value of J_{SHIH} at higher loads and during stable crack growth. Another point of interest is that $J_{EXPERIMENTAL}$ becomes highly contour dependent in the presence of net section yield and before a crack extension of $\Delta a = 1.5$ mm is reached, as shown in Fig. 7(c). This is unexpected in light of previous numerical studies by Shih *et al.* (1981).

Figures 8(a) and (b) show the log–log plots of crack tip u- and v-displacements, respectively, prior to stable crack growth for three angular orientations. Since the objective of this study was to investigate in further detail the validity of the HRR field, only the off-axis orientations, which yielded the most dense moiré fringe patterns, were considered. While the measured and LEFM u- and v-displacements are in reasonable agreement, as expected at this low load, a similar agreement is not observed in the very vicinity of the crack tip.

Due to the uncertainty in the rigid body displacement component in the measured u-displacement, only the slope and not the absolute value of this displacement can be compared with the slope of the LEFM component, i.e. 0.5, and with the slope of the HRR component which is 0.083.

Figures 9(a) and (b) show the variations in the two normal strains, ε_{xx} and ε_{yy}, with crack tip distance r, at three angular orientations of $\theta = 30°$, 45° and 60° prior to stable crack growth. While the ε_{yy} followed the LEFM ε_{yy}, as expected from the results of Fig. 8(b), the ε_{xx} deviated from the LEFM ε_{xx} at $r < 1$ mm in the region of $\theta < 45°$. Such a difference was unexpected since Fig. 8(a) showed that the slope of the log–log plot of the u-displacement was the anticipated LEFM slope of 1/2.

Figures 10(a) and (b) show the log–log plots of the crack tip u- and v-displacements, respectively, at the onset of stable crack growth. The u-displacement continues to maintain its elastic response while the v-displacement is approaching the HRR displacement at about $r = 1$ mm.

Figures 11(a) and (b) show the variations in the two normal strains, ε_{xx} and ε_{yy}, with r at $\theta = 30°$, 45° and 60°. Also plotted, in addition to the corresponding LEFM normal strain, are the HRR strains computed using the measured J-integral values. Despite the increasing size in the plastic region, these results are similar to those in Figs 9(a) and (b) where the LEFM strain field still dominates.

Figures 12(a) and (b), as well as 13(a) and (b), show the log–log plots of the crack tip displacements for a moderate stable crack growth, i.e. $\Delta a = 1.5$ mm and 3.9 mm, respectively. The slope and the value of the v-displacement is now in good agreement with those of the HRR displacement. The slope and the value of u-displacement, however, continues to follow those and the value of the LEFM displacement.

The Q value in these figures represents the absolute value of the difference between the measured and the HRR displacements computed from the measured J values and is not the Q value used by Shih *et al.* (1979). The simplified J–Q theory predicts for a state of *plane stress*, vanishing Q components as per Aravas (1993). Figures 13(a,b) show that the Q components are of the same order as the measured u and v values. The slopes of the Q components for the v-displacement vary from 0 to 0.18 within the region of $r\sigma_0/J < 3$. In the region of $3 < r\sigma_0/J < 10$, the average slope of the Q components for the u and v displacements are approximately 0.9 and 0, respectively.

Figures 14(a) and (b) and Figs 15(a) and (b) show the variations in two crack normal strains, ε_{xx} and ε_{yy}, for moderate crack growths of $\Delta a = 1.5$ and 3.9 mm, respectively. Also plotted are the corresponding HRR strains which were computed by using the experimentally determined J-integral values. In terms of absolute values, the HRR strain grossly over predicts ε_{xx} while it agrees well with the experimental ε_{yy} for $\theta = 60°$ but not so well at $\theta = 30°$ and 45°.

Figure 16 shows the variations in the crack tip opening angle (CTOA), as measured 1 mm from the crack tip, using the coarse and fine grating moiré interferometry data, with the increase in load–line displacement. The CTOA reached a nearly constant value at a crack extension of $\Delta a = 1.5$ mm with a leveled resistance curve thereafter. Since CTOA is related to the maximum strain at the crack tip, this result suggests that CTOA could be a viable ductile fracture parameter. The well known disadvantage is that CTOA cannot be readily measured with a normal testing facility and that it is impractical to determine in complex flaw geometries, such as a surface flaw.

CONCLUSIONS

Limited experimental results involving the crack tip displacement fields in thin aluminum SEN with small stable crack growth showed that the J–Q theory, based on the plane strain form of O'Dowd and Shih (1993), may not be present. On the other hand, the crack tip field of Yang *et al.* (1993) could exist.

For an elastic–plastic fracture analysis of thin plates in the presence of stable crack growth, the present J-integral computation procedures based on Kumar *et al.* (1981) and on a commercial code must be reinvestigated in view of the observed large discrepancies.

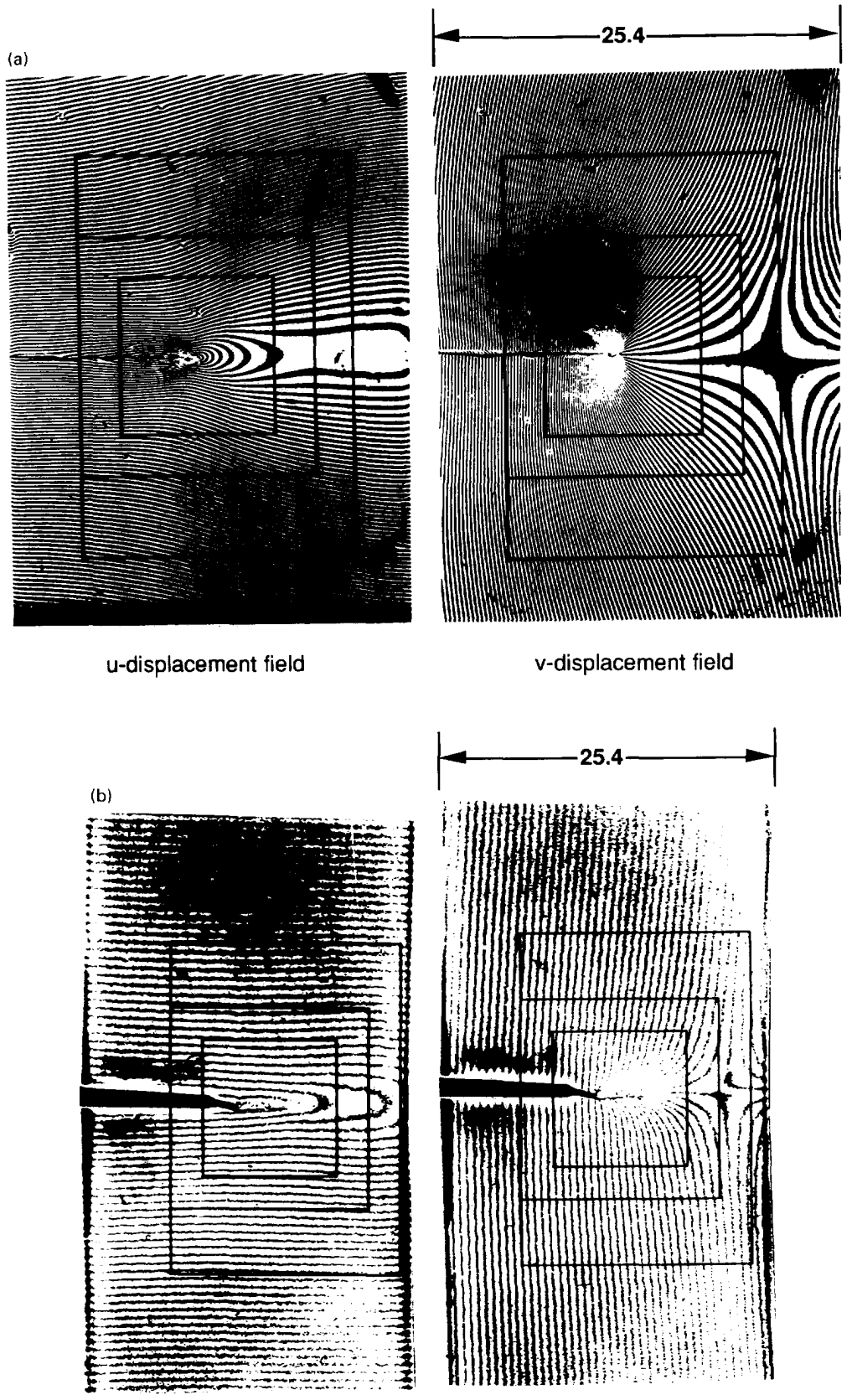

Fig. 6. Moiré interferometry patterns of the 2024-T3 SEN specimen with J contours shown [load = 1134 (N)]: (a) fine grid analysis; (b) coarse grid analysis.

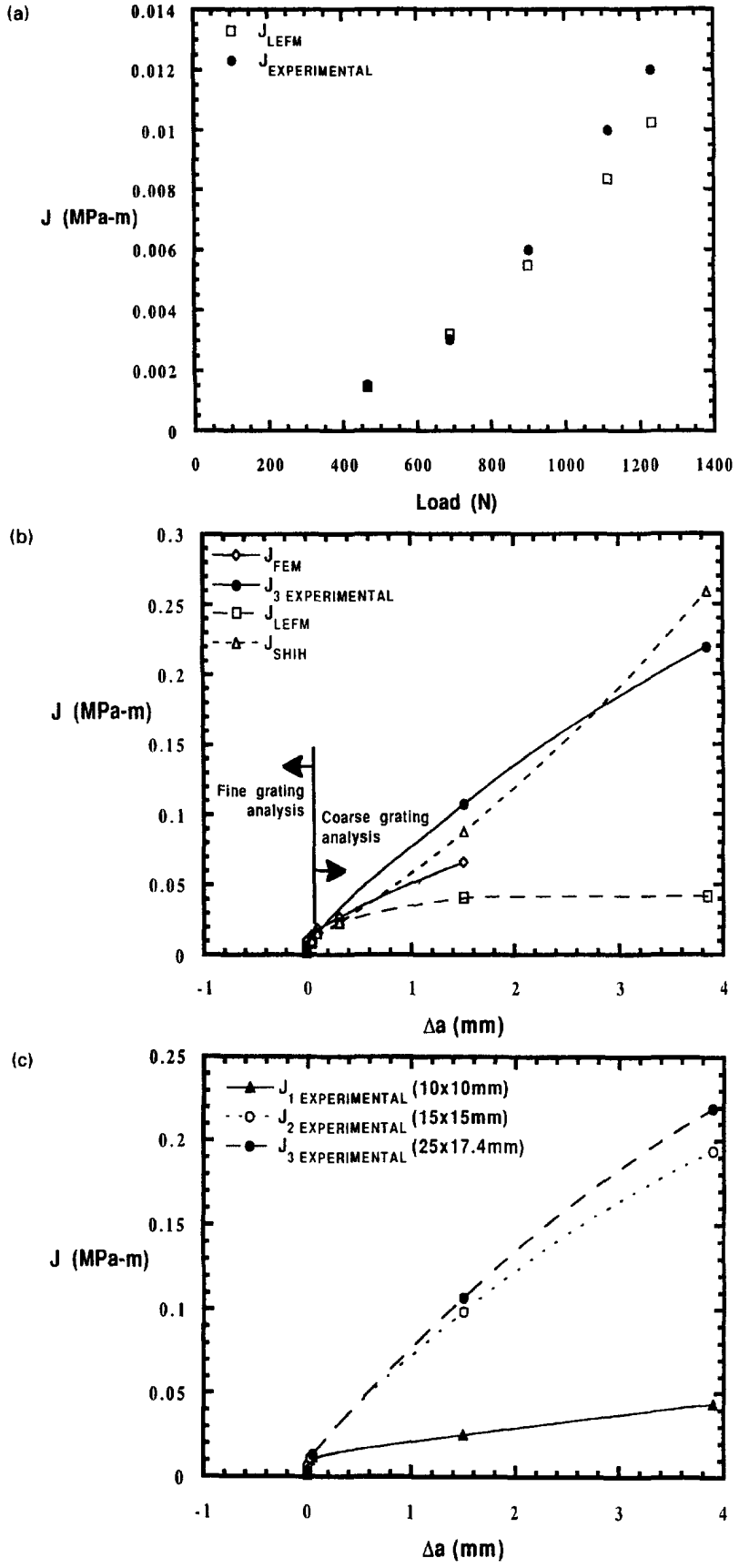

Fig. 7. (a) J-integral values of 2024-T3 SEN specimens prior to stable crack growth; (b) J-integral values of 2024-T3 specimen under stable crack growth; (c) variation in the J-integral values of 2024-T3 specimen under stable crack growth.

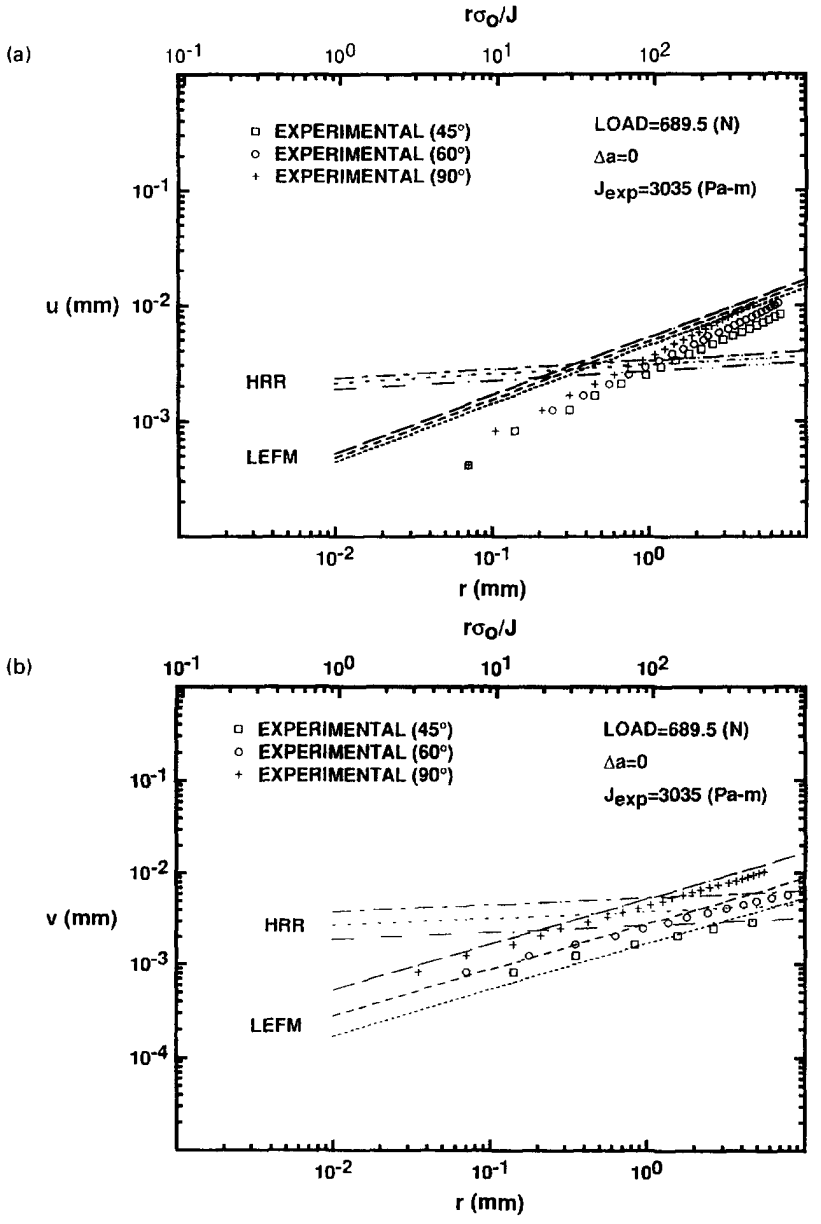

Fig. 8. (a) Crack tip u-displacement of 2024-T3 SEN specimen prior to stable crack growth; fine grating analysis. (b) Crack tip v-displacement of 2024-T3 SEN specimen prior to stable crack growth; fine grating analysis.

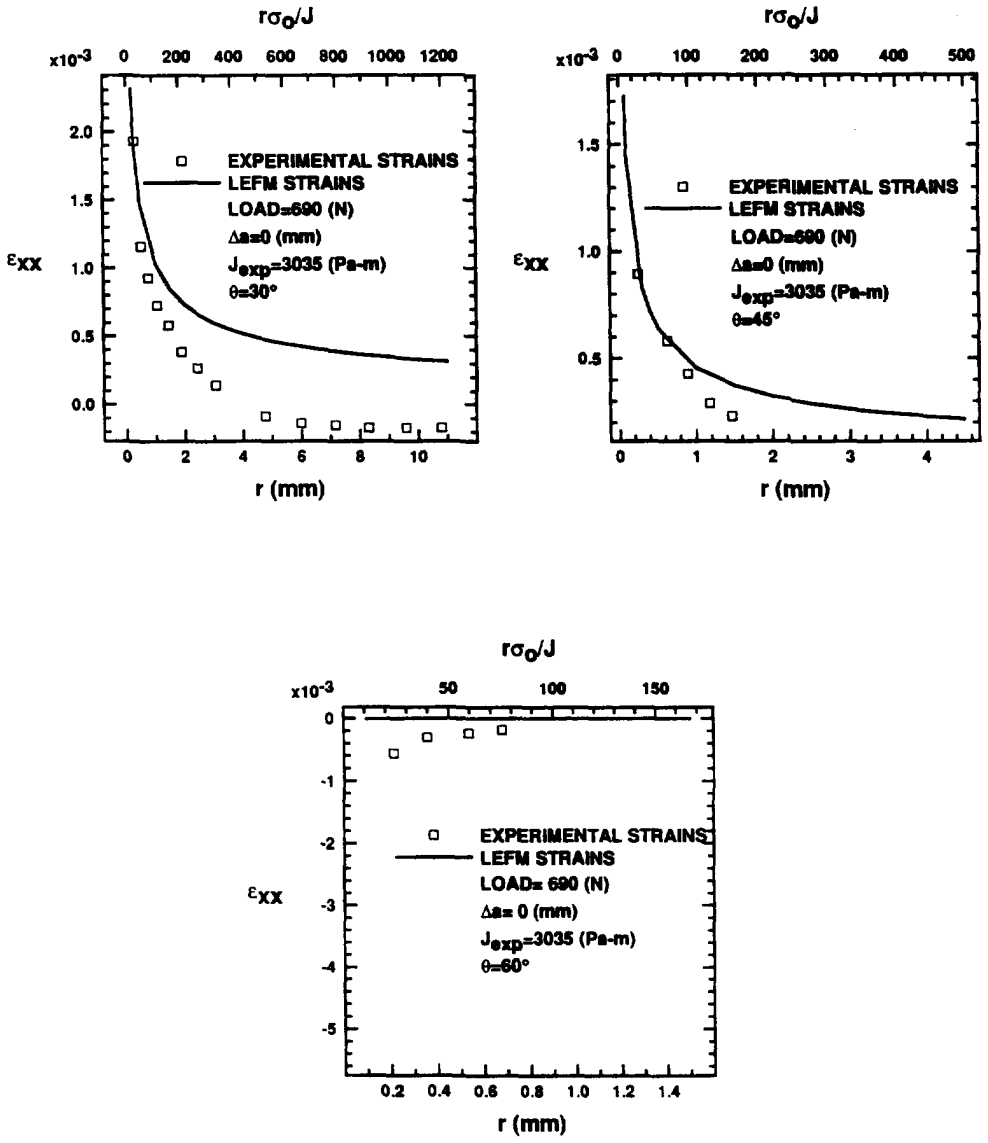

Fig. 9(a). Crack tip ε_{xx} of 2024-T3 SEN specimen prior to stable crack growth ; fine grating analysis.

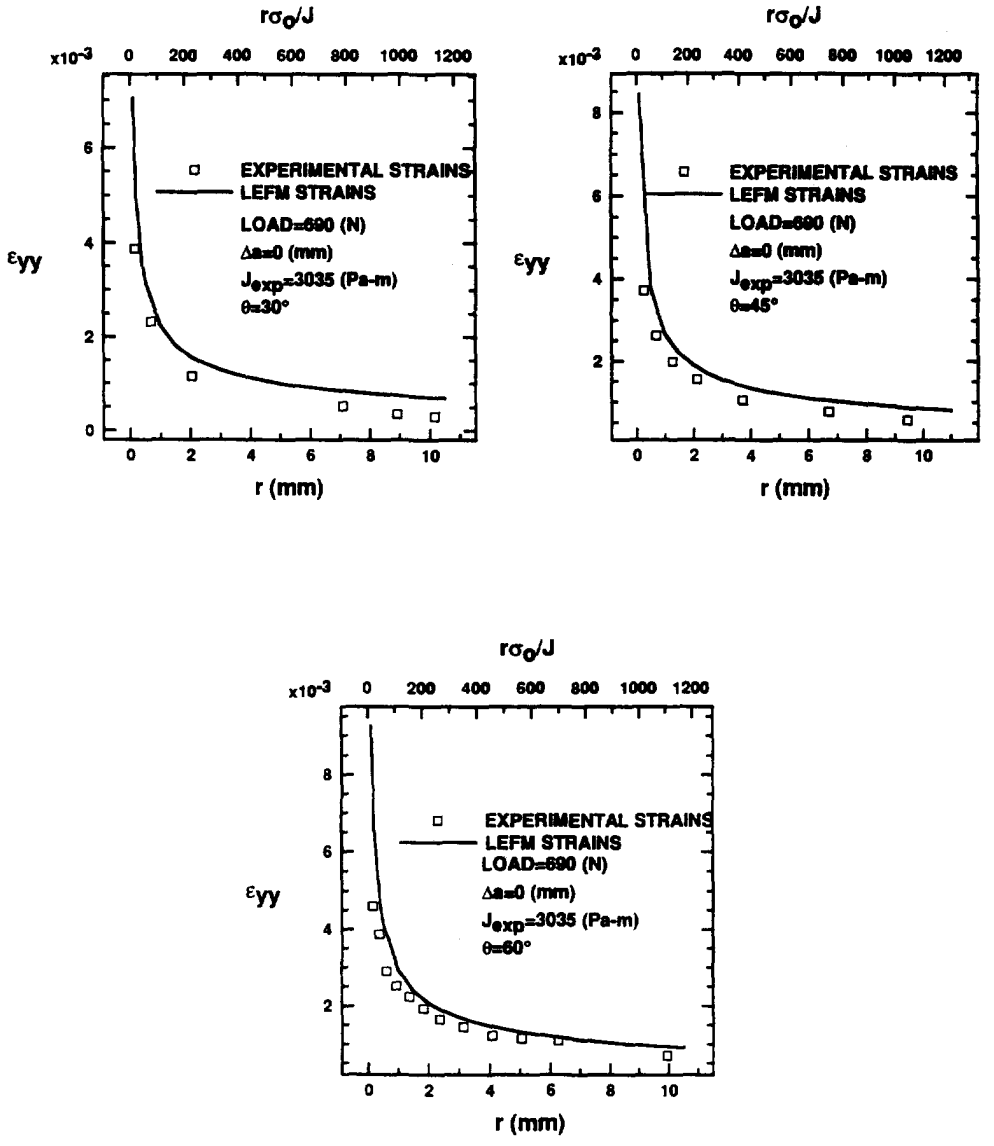

Fig. 9(b). Crack tip ε_{yy} of 2024-T3 SEN specimen prior to stable crack growth; fine grating analysis.

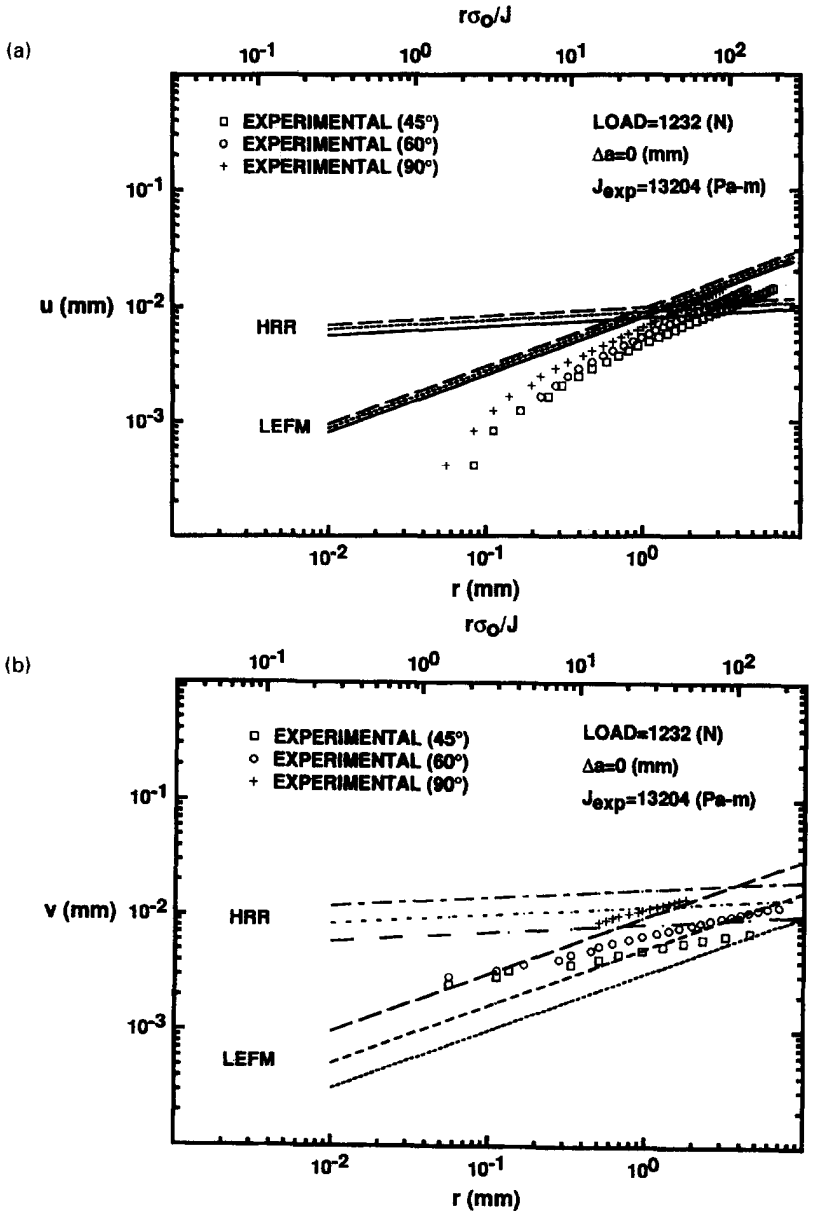

Fig. 10. (a) Crack tip u-displacement of 2024-T3 SEN specimen at the onset of stable crack growth; fine grating analysis. (b) Crack tip v-displacement of 2024-T3 SEN specimen at the onset of stable crack growth; fine grating analysis.

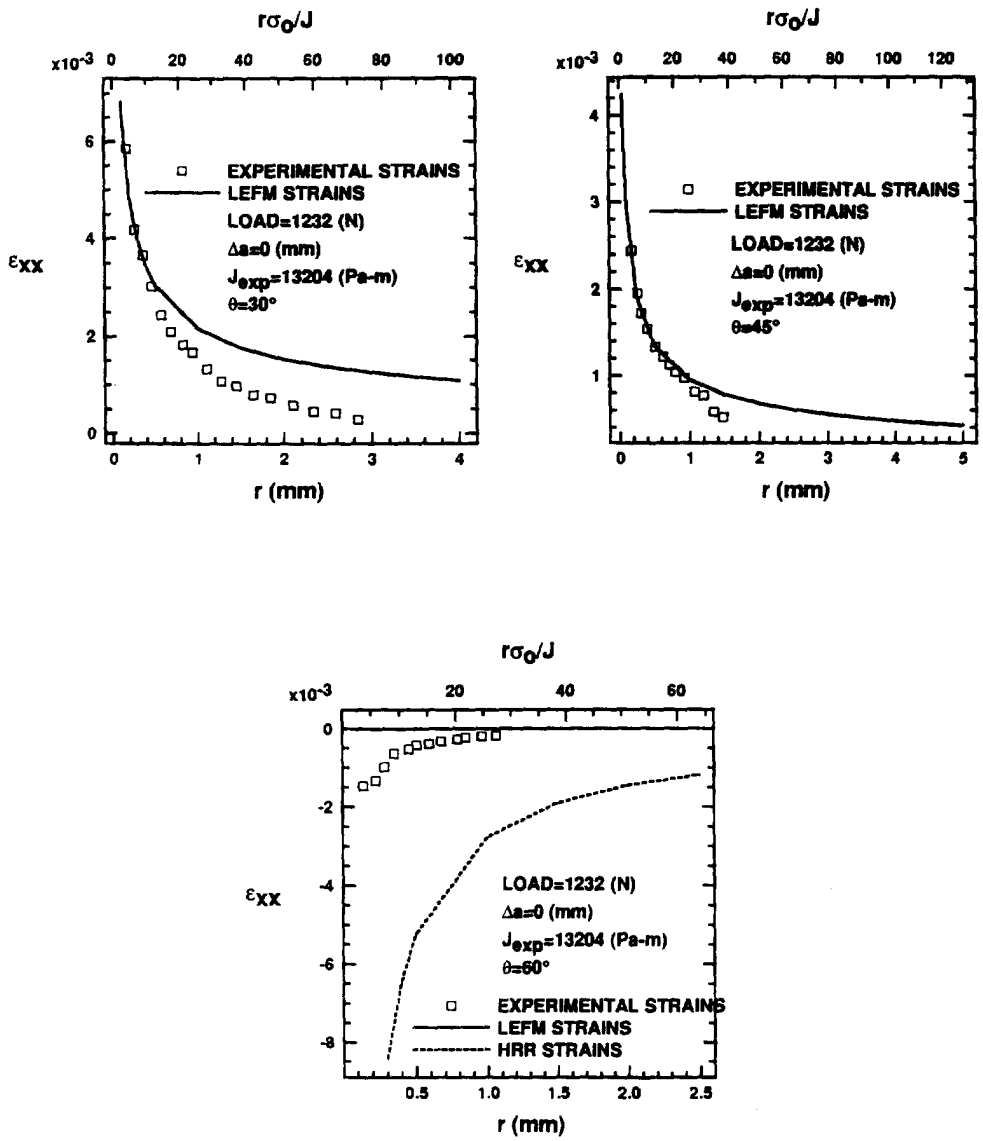

Fig. 11(a). Crack tip ε_{xx} of 2024-T3 SEN specimen at the onset of stable crack growth; fine grating analysis.

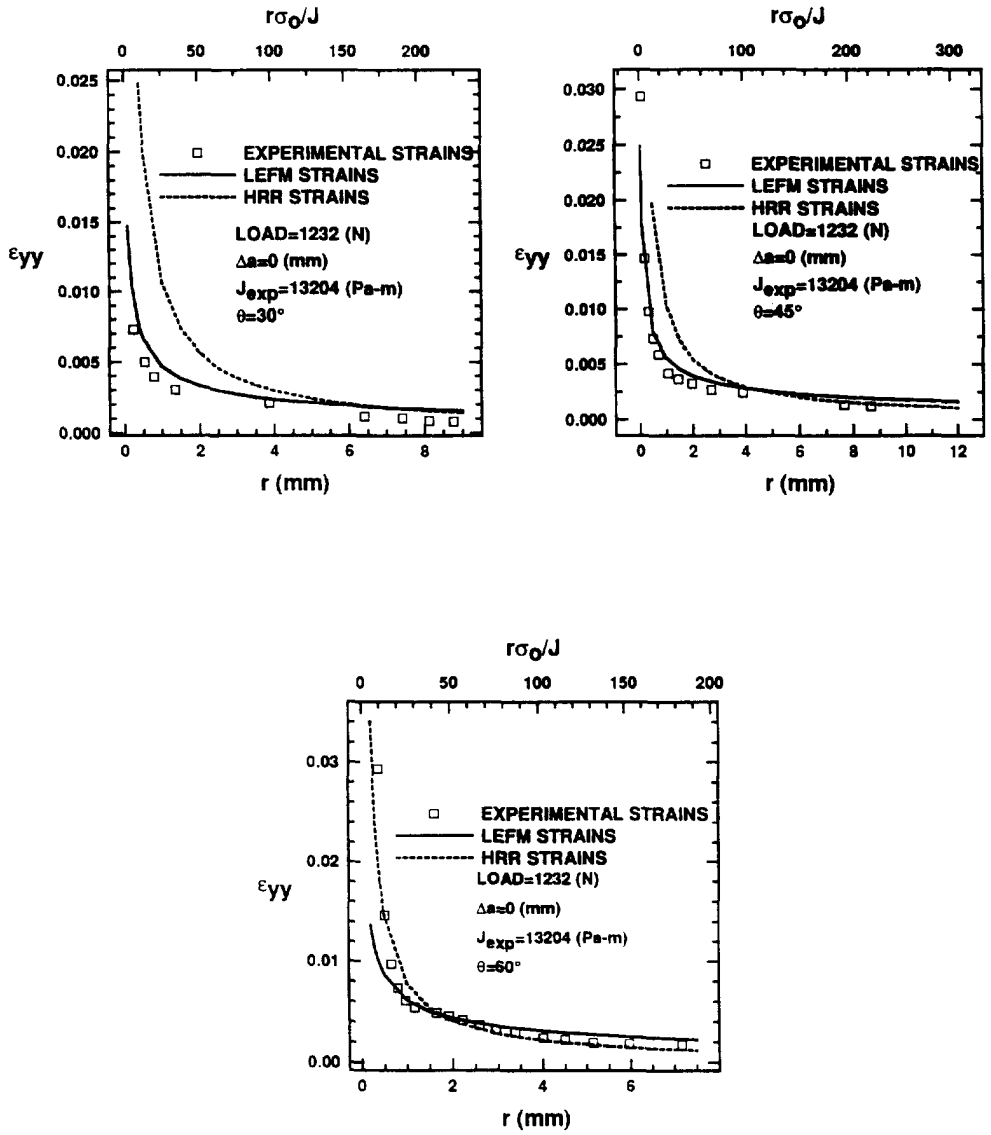

Fig. 11(b). Crack tip ε_{yy} of 2024-T3 SEN specimen at the onset of stable crack growth; fine grating analysis.

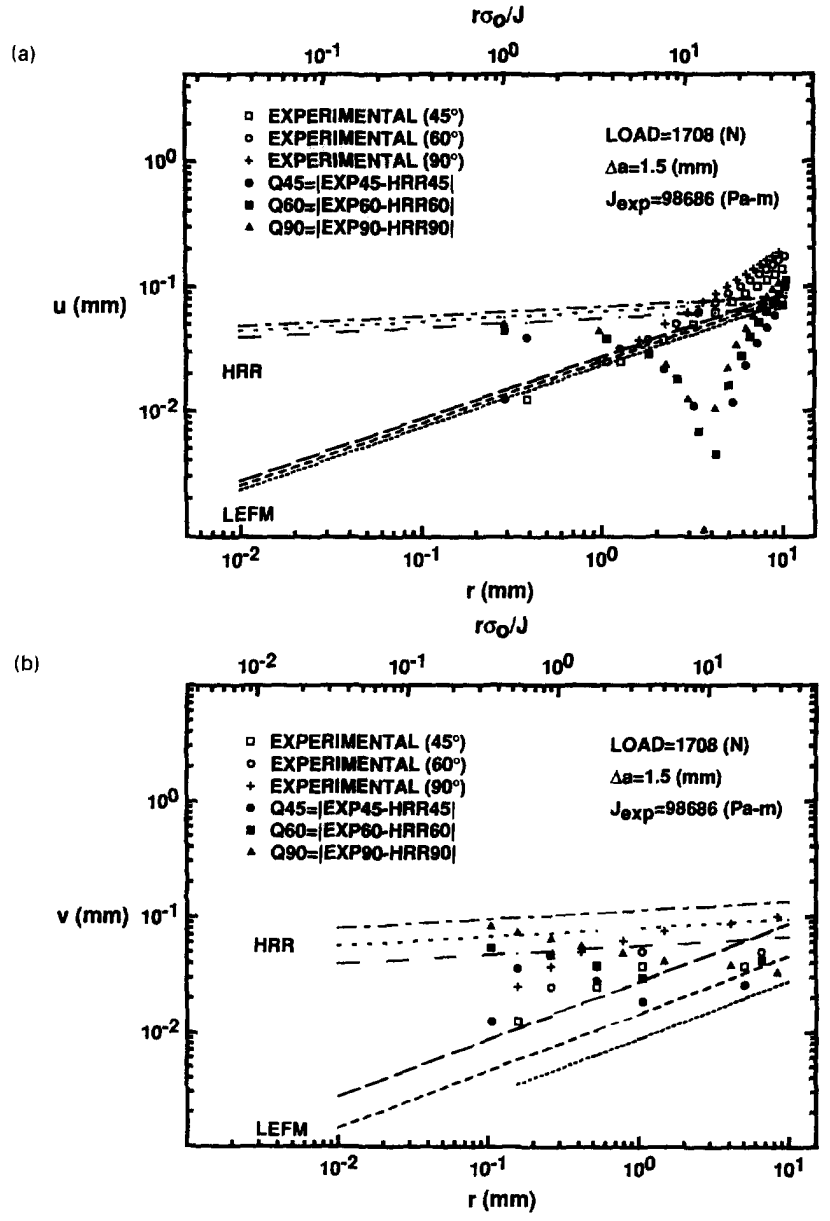

Fig. 12. (a) Crack tip u-displacement of 2024-T3 SEN specimen with small crack growth; coarse grating analysis. (b) Crack tip v-displacement of 2024-T3 SEN specimen with small crack growth; coarse grating analysis.

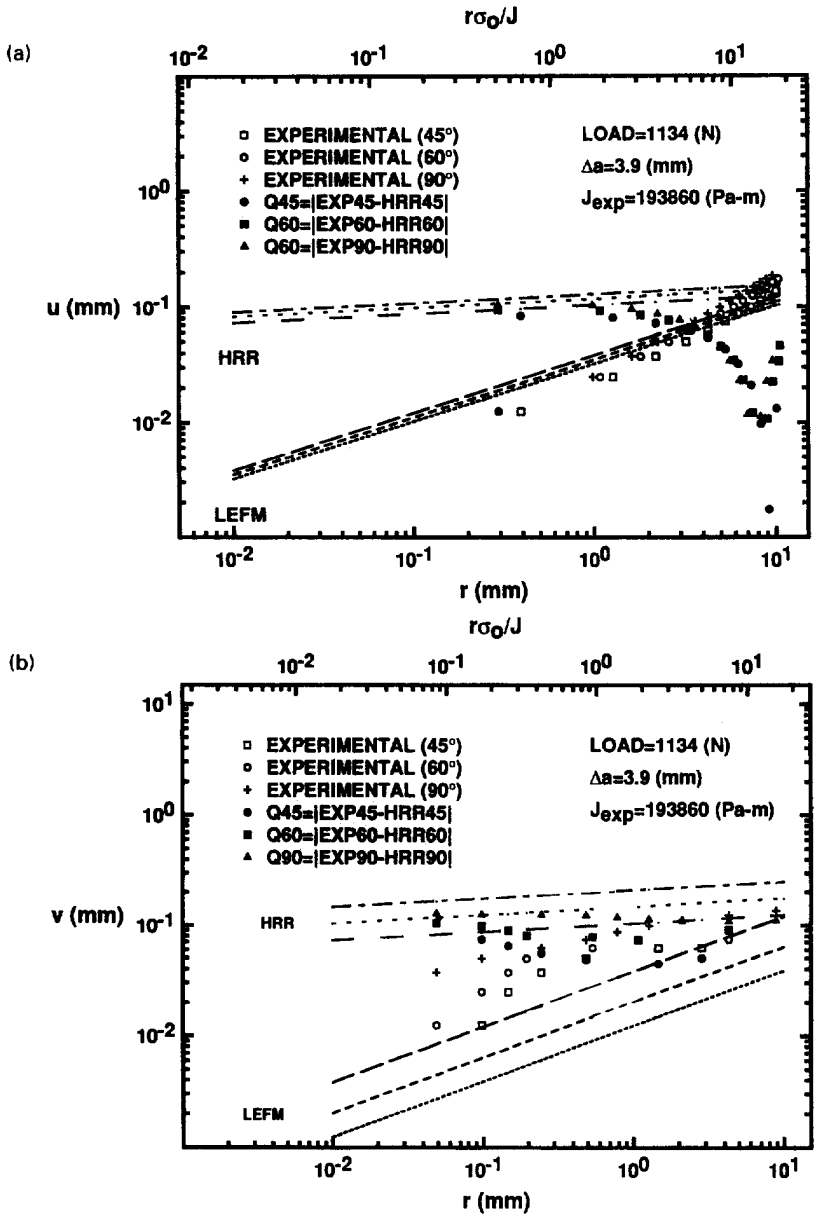

Fig. 13. (a) Crack tip u-displacement of 2024-T3 SEN specimen with moderate stable crack growth; coarse grating analysis. (b) Crack tip v-displacement of 2024-T3 SEN specimen with moderate stable crack growth; coarse grating analysis.

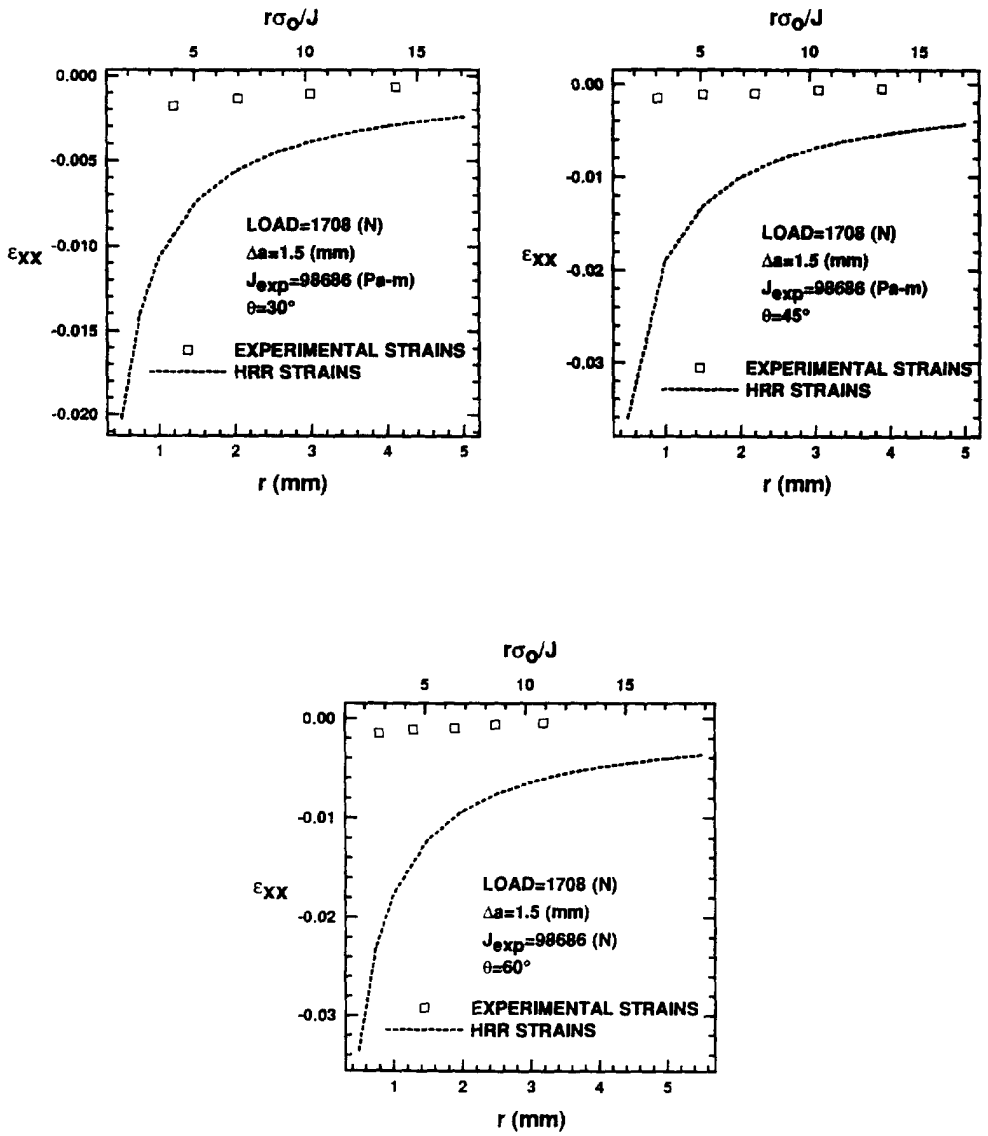

Fig. 14(a). Crack tip ε_{xx} of 2024-T3 SEN specimen with small stable crack growth; coarse grating analysis.

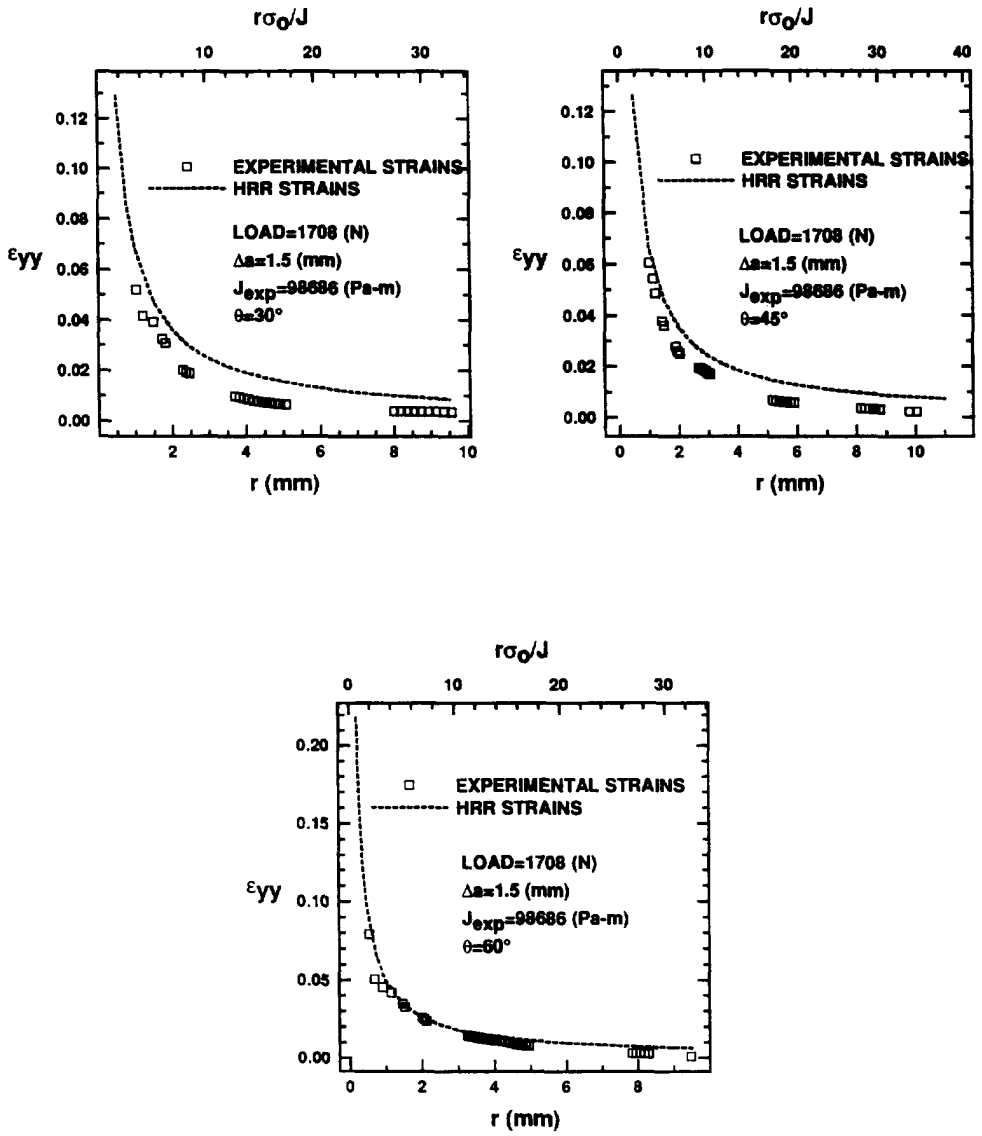

Fig. 14(b). Crack tip ε_{yy} of 2024-T3 SEN specimen with small stable crack growth; coarse grating analysis.

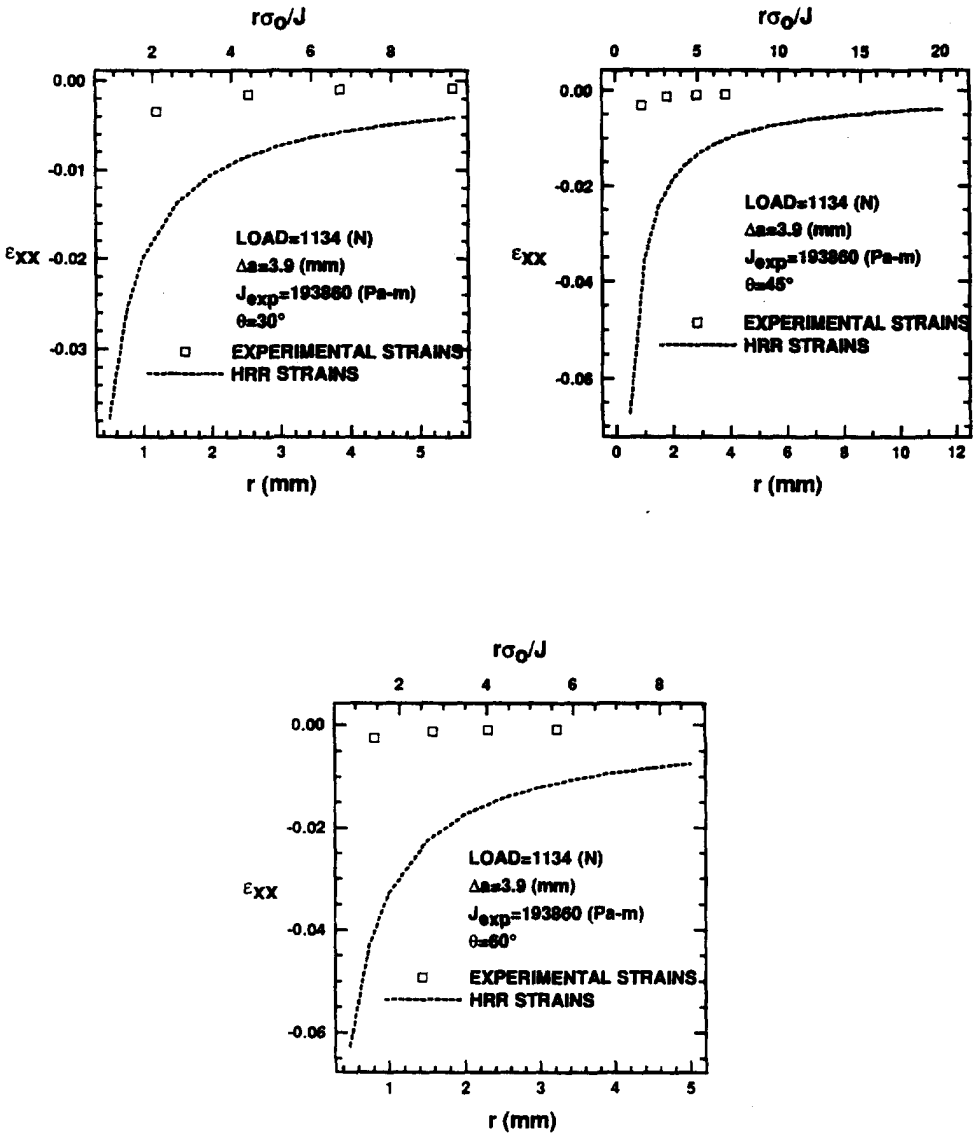

Fig. 15(a). Crack tip ε_{xx} of 2024-T3 SEN specimen with moderate stable crack growth; coarse grating analysis.

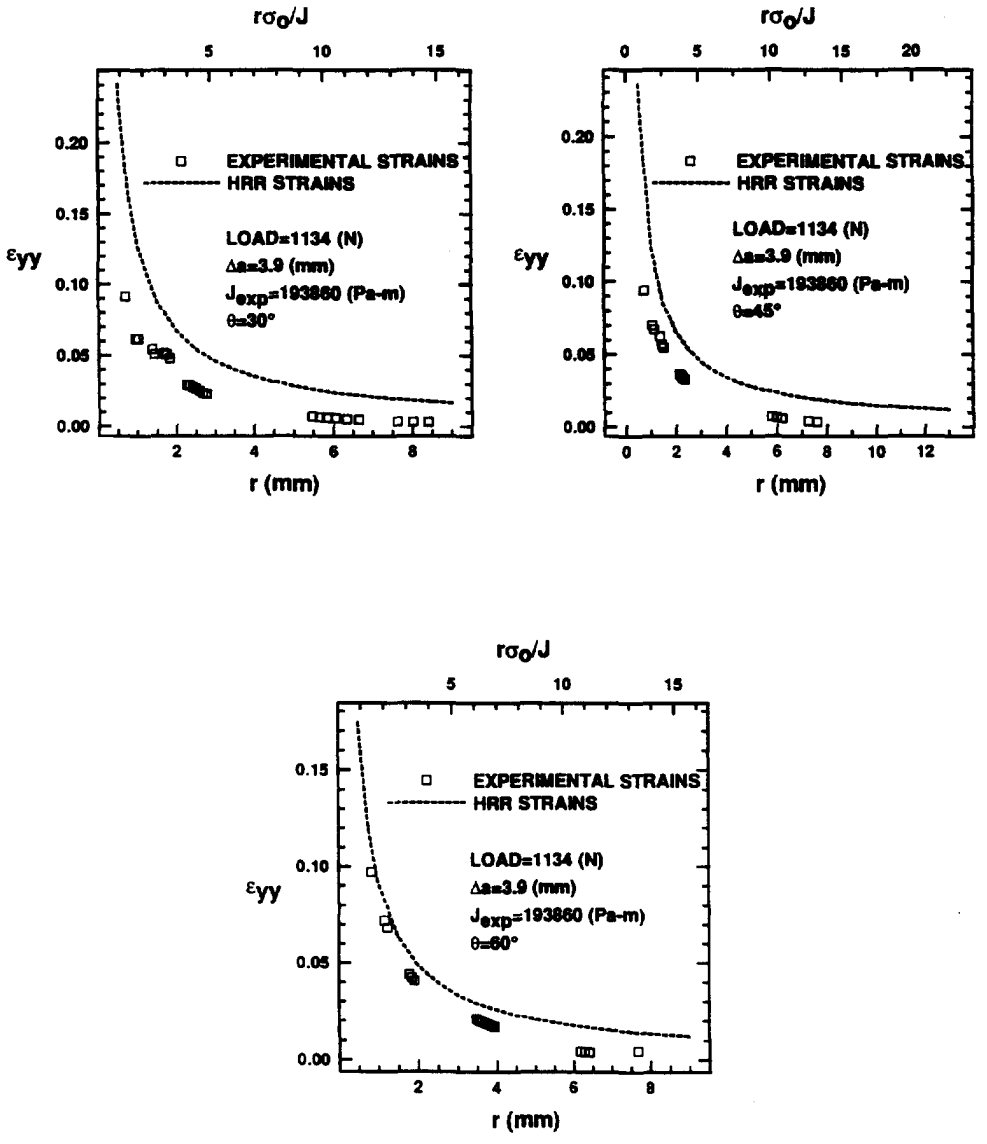

Fig. 15(b). Crack tip ε_{yy} of 2024-T3 SEN specimen with moderate stable crack growth; coarse grating analysis.

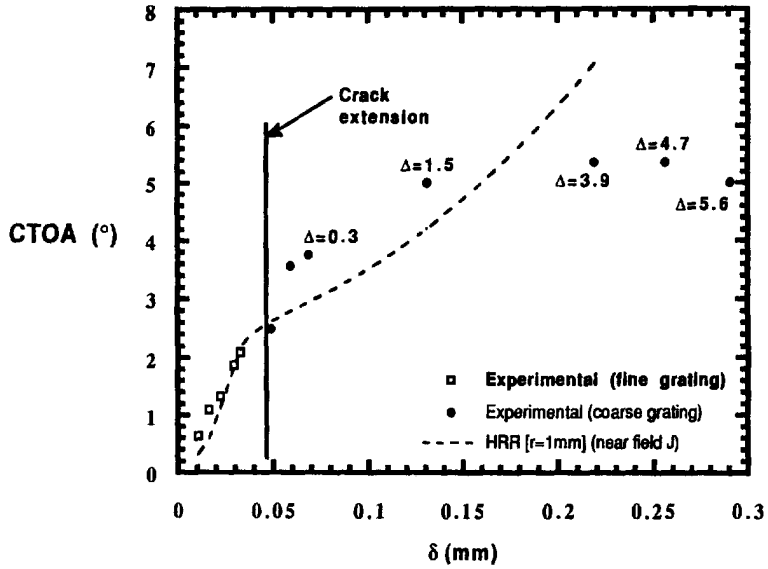

Fig. 16. CTOA variation with increasing load–line displacement.

Preliminary results show that the CTOA could be a viable ductile fracture parameter for stable crack growth and ductile fracture.

Acknowledgements—This research was supported by the Office of Naval Research under ONR Contract N00014-89-J-1276. The authors are indebted to Dr Yapa D. S. Rajapakse for his support during the course of this investigation.

REFERENCES

Aravas, N. (1993). Private communication.

Betegon, C. and Hancock, J. W. (1991). Two-parameter characterization of elastic–plastic crack tip field. *ASME J. Appl. Mech.* **58,** 104–110.

Chao, Y.-J. (1993a). On a single parameter controlled fracture of solids under plane stress conditions. *Int. J. Fract.* **62,** R7–10.

Chao, Y. J. (1993b). Private communication.

Dadkhah, M. S. and Kobayashi, A. S. (1990). Further studies in the HRR field of a moving crack ; an experimental analysis. *J. Plasticity* **6,** 636–650.

Dadkhah, M. S. and Kobayashi, A. S. (1994). Two-parameter crack tip stress field, associated with stable crack growth in a thin plate. To be published in *Fract. Mech. 24th Symp.* ASTM.

Dadkhah, M. S. Kobayashi, A. S. and Morris, W. L. (1992). Crack tip displacement fields and J_R curves of four aluminum alloys. *Fract. Mech. 22nd Symp.* (Edited by S. N. Atluri, J. C. Newman, Jr, I. S. Raju and J. S. Epstein), Vol. II, pp. 135–153. ASTM STP 1131.

Guo, Z. K. and Kobayashi, A. S. (1994). Simultaneous measurement of U and V displacement fields by moiré interferometery. *Exp. Tech.* **17**(5), 21–23.

Hareesh, T. V. and Chiang, F. P. (1988). Integrated experimental-finite element approach for studying elastic–plastic crack tip fields. *Engng Fract. Mech.* **31**(3), 451–461.

Hom, G., Sutton, M. A. and Chao, Y. J. (1994). A study of crack tip deformation fields in thin sheets by computer vision. *Exp. Mech.* **34**(2), 125–140.

Hutchinson, J. W. (1968). Plastic stress and strain fields at a crack tip. *J. Mech. Phys. Solids* **16,** 13–31.

Ifju, P. and Post, D. (1991). Zero-thickness specimen grating for moiré interferometry. *Exp Tech.* **15**(2), 45–47.

Kang, B. S. and Kobayashi, A. S. (1988). J-estimation procedure based on moiré interferometry data. *ASME J. Pressure Vessel Tech.* **110,** 291–300.

Kirk, M. T., Kippenhoefer, K. C. and Shih, C. F. (1993). Effect of constraint on specimen dimensions needed to obtain structurally relevant toughness measures. In *Constraint Effects in Fracture* (Edited by E. M. Hackett, K.-H. Schwalbe and R. H. Dodds, Jr), pp. 79–103. ASTM STP 1171.

Kumar, V., German, M. D. and Shih, C. F. (1981). An engineering approach for elastic–plastic fracture analysis. Electric Power Research Institute Topical Research, NP-1931, Research Project 1237-1.

Li, Y. and Wang, X. (1986). Higher-order asymptotic field of tensile plane-strain nonlinear crack problems. *Sci. Sin.* **XXIX,** 941–955.

May, G. B., Wang, F. X. and Kobayashi, A. S. (1993). Two-parameter crack tip field associated with stable crack growth in a thin plate—a hybrid analysis. *Adv. Tech. Expl Mech. JSME,* 19–24.

O'Dowd, N. P. and Shih, C. F. (1991). Family of crack-tip fields characterized by a triaxiality parameter—I. Structure of fields. *J. Mech. Phys. Solids* **39,** 989–1015.

O'Dowd, N. P. and Shih, C. F. (1992). Family of crack-tip fields characterized by a triaxiality parameter. Part II—Structure fields. *J. Mech. Phys. Solids* **40,** 939–963.

O'Dowd, N. P. and Shih, C. F. (1993). Two-parameter fracture mechanics theory and applications. NUREG/CR-5958, CDNSWS/SME-CR-16-92, Brown University.

Post, D. (1993). Moiré Interferometry. In *Handbook on Experimental Mechanics*, 2nd revised edition (Edited by A. S. Kobayashi), pp. 297–364. VCH Publishers.

Rice, J. R. (1968). A path independent integral and the approximate analysis of strain concentrations by notches and cracks. *ASME J. Appl. Mech.* **351,** 379–386.

Rice, J. R. and Rosengren, G. F. (1968). Plane strain deformation near a crack tip in a power hardening material. *J. Mech. Phys. Solids* **16,** 1–12.

Schultheisz, C. A. (1991). Comparison of experimental and computational crack-tip deformations using moiré interferometry and finite elements. Ph.D. thesis, California Institute of Technology.

Sharma, S. M. and Aravas, N. (1991). Determination of higher order terms in asymptotic crack tip solutions. *J. Mech. Phys. Solids* **39,** 1043–1072.

Shih, C. F. (1983). Tables of Hutchinson–Rice–Rosengren singular field quantities. MRL-E-147, Brown University.

Shih, C. F., de Lorenzi, H. G. and Andrews, W. R. (1979). Studies on crack initiation and stable crack growth. *Elastic–Plastic Fracture* (Edited by J. D. Landes, J. A. Begley and G. A. Clarke), pp. 65–120. ASTM STP 668.

Sivaneri, N. T., Xie, Y. P. and Kang, B. S.-J. (1991). Elastic–plastic crack-tip field numerical analysis integrated with moiré interferometry. *Int. J. Frac.* **49,** 291–303.

Tada, H., Paris, P. C. and Irwin, G. R. (1973). *The Analysis of Cracks Handbook*. Del Research Corp., Hillertown, PA.

Wang, Y. Y. (1993). On the two-parameter characterization of elastic–plastic crack-front fields in surface-cracked plates. In *Constraint Effects in Fracture* (Edited by E. M. Hackett, K. H. Schwalbe and R. H. Dobbs), pp. 120–138. ASTM STP 1171.

Xia, L. and Wang, T. C. (1993). Higher-order analysis of crack tip fields in elastic power-law hardening materials. *J. Mech. Phys. Solids* **41,** 665–687.

Yang, S., Chao, Y. J. and Sutton, M. A. (1993). Higher order asymptotic crack tip fields in a power-law hardening material. *Engng Fract. Mech.* **45**(1), 1–20.